IJMMM
International Journal of
Minerals, Metallurgy and Materials
矿物冶金与材料学报 (英文版)

Preparation of Al_2O_3–SiO_2 composite aerogels and their Cu^{2+} absorption properties

Xiao-guang Liu, Qiu-shuo Mao, Yue Jiang, Yan Li, Jia-lin Sun, and Fei-xue Huang

Cite this article as:
Xiao-guang Liu, Qiu-shuo Mao, Yue Jiang, Yan Li, Jia-lin Sun, and Fei-xue Huang, Preparation of Al_2O_3–SiO_2 composite aerogels and their Cu^{2+} absorption properties, *Int. J. Miner. Metall. Mater.*, 28(2021), No. 2, pp. 317-324. https://doi.org/10.1007/s12613-020-2111-3

View the article online at SpringerLink or IJMMM Webpage.

Articles you may be interested in

Yi-fan Zhang, Zhen Ji, Ke Chen, Cheng-chang Jia, Shan-wu Yang, and Meng-ya Wang, Preparation and radar-absorbing properties of Al_2O_3/TiO_2/Fe_2O_3/Yb_2O_3 composite powder, *Int. J. Miner. Metall. Mater.*, 24(2017), No. 2, pp. 216-221. https://doi.org/10.1007/s12613-017-1398-1

Wei Liu, Qing-he Zhao, and Shuan-zhu Li, Relationship between the specific surface area of rust and the electrochemical behavior of rusted steel in a wet-dry acid corrosion environment, *Int. J. Miner. Metall. Mater.*, 24(2017), No. 1, pp. 55-63. https://doi.org/10.1007/s12613-017-1378-5

Peng Zhou, Jun-hong Chen, Meng Liu, Peng Jiang, Bin Li, and Xin-mei Hou, Microwave absorption properties of SiC@SiO_2@Fe_3O_4 hybrids in the 2-18 GHz range, *Int. J. Miner. Metall. Mater.*, 24(2017), No. 7, pp. 804-813. https://doi.org/10.1007/s12613-017-1464-8

Zhi-yuan Chen, Liu-zhen Bian, Zi-you Yu, Li-jun Wang, Fu-shen Li, and Kuo-Chih Chou, Effects of specific surface area of metallic nickel particles on carbon deposition kinetics, *Int. J. Miner. Metall. Mater.*, 25(2018), No. 2, pp. 226-235. https://doi.org/10.1007/s12613-018-1565-z

Franco Mayanglambam and Mark Russell, Reusing oxide-based pulverised fly ash and medical waste particles to develop electroless nickel composite coatings (Ni–P/fly ash and Ni–P/SiO_2–Al_2O_3), *Int. J. Miner. Metall. Mater.*, 27(2020), No. 8, pp. 1147-1156. https://doi.org/10.1007/s12613-020-2071-7

Wei Li, Nan Wang, Gui-qin Fu, Man-sheng Chu, and Miao-yong Zhu, Effect of Cr_2O_3 addition on the oxidation induration mechanism of Hongge vanadium titanomagnetite pellets, *Int. J. Miner. Metall. Mater.*, 25(2018), No. 4, pp. 391-398. https://doi.org/10.1007/s12613-018-1583-x

IJMMM WeChat

QQ author group

International Journal of Minerals, Metallurgy and Materials
Volume 28, Number 2, February 2021, Page 317
https://doi.org/10.1007/s12613-020-2111-3

Preparation of Al_2O_3–SiO_2 composite aerogels and their Cu^{2+} absorption properties

*Xiao-guang Liu*1), *Qiu-shuo Mao*1), *Yue Jiang*1), *Yan Li*1), *Jia-lin Sun*1), *and Fei-xue Huang*2)

1) School of Materials Science and Engineering, University of Science and Technology Beijing, Beijing 100083, China
2) Fundamental Experimental Centre of Nature Science, University of Science and Technology Beijing, Beijing 100083, China

(Received: 11 November 2019; revised: 30 May 2020; accepted: 1 June 2020)

Abstract: In order to remediate heavy metal ions from waste water, Al_2O_3–SiO_2 composite aerogels are prepared via a sol–gel and an organic solvent sublimation drying method. Various characterisation techniques have been employed including X-ray diffraction (XRD), Fourier transform infrared spectrometry (FTIR), scanning electron microscope (SEM), Energy-dispersion X-ray spectroscopy (EDX), Brunauer–Emmett–Teller (BET) N_2 adsoprtion isotherm, and atomic absorption spectrometer (AAS). XRD and FTIR suggest that the aerogels are composed of mainly Al_2O_3 and minor SiO_2. They have a high specific surface area (827.544 m^2/g) and high porosity (86.0%) with a pore diameter of ~20 nm. Their microstructures show that the distribution of Al, Si, and O is homogeneous. The aerogels can remove ~99% Cu^{2+} within ~40 min and then reach the equilibrium uptake (~69 mg/g). Preliminary calculations show that the Cu^{2+} uptake by the aerogels follows pseudo second-order kinetics where chemical sorption may take effect owing largely to the high surface area, high porosity, and abundant functional groups, such as Al–OH and Si–OH, in the aerogel network. The prepared aerogels may serve as efficient absorbents for Cu^{2+} removal.

Keywords: heavy metal ion; aerogel; absorption; organic solvent sublimation drying; specific surface area; porosity

1. Introduction

Wastewater from chemical emissions, oil spillages, and biomedical pollutants poses a serious threat to humans and the environment. Hence, wastewater remediation is highly important. Toxic heavy metal ions (Cu^{2+}, Pb^{2+}, Cd^{2+}, Zn^{2+}, Hg^{2+}, Ni^{2+}, and $Cr_2O_7^{2-}$) are nondegradable and are carcinogenic to humans [1]. Therefore, heavy metal ions must be properly treated before being discharged to the environment. Conventional methods of wastewater treatment are filtration [2], precipitation [3], ion exchange [4], electrochemical treatments [5], and photocatalysis [6–7]. Despite their efficiency in the removal of heavy metal ions, these methods suffer from various limitations. For instance, the chemical precipitation routes show low removal efficiency and sometimes leave large amounts of sludge after use [3]. In addition, photocatalysis produces undesirable by-products, such as Cr(III) ions from Cr(VI) reduction, and thus needs a secondary treatment [6–7]. Meanwhile, ion exchange suffers from high pH dependencies [4]. Moreover, membrane filtration and electrochemical treatment are expensive to become commercially available [2,5]. With these considerations, absorption is still a cost-effective way to remove heavy metal ions (even at trace concentration). Other advantages of this method include easy implementation, simple design, none/less secondary products, effective cost, and being recyclable [8], enabling its wide applications.

To date, extensive absorbent materials, such as active carbon, zeolite [9], and organic resins [10], have been studied. However, active carbon, although cheap, is limited by its low absorption capacities and nonselectivity. The organic resin is almost nonrecyclable, nonregenerative, and thermally unstable [8,10]. Recent studies have reported that nanomaterials are promising in removing heavy metal ions [11–12] but are expensive and complex at processing [13]. Furthermore, they tend to agglomerate [12], which severely hinders their wide applications. Consequently, efficient absorbents with nanostructures and bulk structures are still highly in demand. Aerogels are excellent materials bridging nanostructures into intact bulk materials while preventing nanomaterial from aggregation [14]. Recently, Maleki has reviewed various aerogels [1], including inorganic [15–25], organic [26–27], car-

---

Corresponding author: Xiao-guang Liu E-mail: liuxg@ustb.edu.cn bon [28–31], semiconductor chalcogenide [32–33], and natural based aerogels [34–36], which have been used in environmental protection. Nanostructured Al_2O_3–SiO_2 shows high efficiencies in removing heavy metal ions because of its high surface area and rich surface functional groups containing oxygen [37]. However, retaining the intact bulk shape while maintaining the excellent dispersion of individual Al_2O_3/SiO_2 nanoparticles is challenging. On the one hand, the hydrolysis rate and pH value are challenging to adjust, especially when mixing two sols (e.g., SiO_2 and Al_2O_3 ones). This phenomenon could lead to severe phase separations and nonhomogeneity and thus poor absorption. A similar but simpler propylene oxide (PO)-assistant sol–gel method (without using various dry controlling agents, such as formamide [38–39]) could be employed to overcome the aforementioned problems. On the other hand, although supercritical [34] and freeze drying [35–36] have been explored for this purpose, the former is expensive and dangerous because of the high pressure involved [21], and the latter induces severe cracks. Consequently, a new drying method needs to be developed urgently. A recent study has shown that an organic solvent sublimation drying (OSSD) method [21] can keep the aerogel intact and retain the surface area by minimizing the capillary forces in the channels/pores of a wet gel [21].

In this work, we designed an aerogel structure to assemble the Al_2O_3/SiO_2 nanoparticles and to obtain high surface area by using an improved sol–gel and OSSD technique. The improvements are that almost no drying agents (as listed in reference [38–39]) are used, and the drying period can be shorten to 3 d. In this way, the dispersion (without agglomeration) of Al_2O_3–SiO_2 nanostructures is improved while the intact bulk aerogel structure is mostly maintained through a simplified PO-assistant sol–gel method and a facile OSSD drying technique. Furthermore, Cu^{2+}, a common heavy metal ion in industrial wastewater and a major pollutant, is chosen as the model heavy metal ion to test the absorption properties of the aerogels in this work.

2. Materials and methods

A clear Al_2O_3 sol was prepared through mixing 17 mL (0.3 mol) C_2H_5OH, 15.2 mL (0.86 mol) demineralized water, and 4.83 g (0.02 mol) $AlCl_3\cdot 6H_2O$ at 50°C for 30 min under magnetic stirring. Similarly, a SiO_2 sol was prepared via reacting 0.56 mL (0.0025 mol) Tetraethyl orthosilicate (TEOS) with 0.18 mL (0.01 mol) demineralized water at 50°C for 90 min. The two sols were subsequently mixed uniformly, in which PO (0.16 mol) was added at 50°C for 10 min to allow the cross-linking reaction. The sol was changed to a wet gel, which was stored at room temperature for 2 h and aged in C_2H_5OH for 24 h. Subsequently, a gradual solvent exchange procedure was conducted in 3 d [21] (day 1: 100wt% C_2H_5OH, day 2: 50wt% C_2H_5OH and 50wt% acetonitrile, day 3: 100wt% acetonitrile), which is shorter than the usual 5-d scheme used in [21] and is an improved OSSD method. It was then dried in a vacuum chamber in accordance with the OSSD protocol at 80–100 Pa and 50°C under the same mechanism [21]. The as-dried gel was heated at 600–1200°C for 2 h in a muffle furnace before further characterizations.

The as-prepared sample was identified using X-ray diffraction (XRD) at 30 mA and 40 kV (XRD TTRIII, Rigaku, Japan) with Ni-filtered Cu K_α radiation. Its molecular structures and chemical composition were characterized using Fourier transform infrared (FTIR) spectrometry in transmission mode (SHIMAZDU spectrometer model IRAFFINITY-1, FTIR-8400S). The porosity, pore size distribution, specific surface areas, and absorption–desorption loops of the sample were measured using a QuantaChrome instrument (QuadraSorb SI). In addition, the microstructures of the sample were observed via a field-emission scanning electron microscopy (SEM, Zeiss SUPRA55, Germany) and a transmission electron microscope (TEM, JEM 2100, JOEL, Japan). Finally, an absorption experiment was performed where 100 mL of $CuSO_4$ solution containing (60 mg/L Cu^{2+}) was used as the model solution, and its supernatant was taken out at various times after its contact with the as-prepared aerogel. The Cu^{2+} concentration of the supernatant was measured using an atomic absorption spectrometer (MKIIM6, Thermo, USA), and the Cu^{2+} concentration data were recorded and plotted with contact time.

3. Results and discussion

3.1. Phase characterization

The XRD patterns (Fig. 1) revealed that the as-prepared samples contain alumina (JCPDS card No. [04-0875]) at 600 and 800°C and some minor amorphous or less crystallized phases appearing as a bump at the 2θ angles of 20°–30°. When the temperature was increased to 1000°C, the Al_2O_3 peaks became sharper and narrower, whereas the amorphous phase disappeared probably because it reacted with or doped into Al_2O_3 upon the heat treatment. When the temperature was further increased to 1200°C, mullite (JCPDS card No. [02-0431]) was detected. Therefore, the unidentified phase may be SiO_2 because a similar bump at the identical 2θ angles (20°–30°) in the corresponding XRD profiles was previously proven to be SiO_2 [22,38]. The existence of Si–O–Si or Si–OH in the network below 1000°C was then confirmed.

3.2. FTIR observation

FTIR spectroscopy was performed on various samples, including the as-dried, 800°C-heated and 1000°C-heated samples, to verify the formation of Si–O–Si, Al–O–Si, or Si–OH bond in the as-prepared aerogels (Fig. 2). The as-

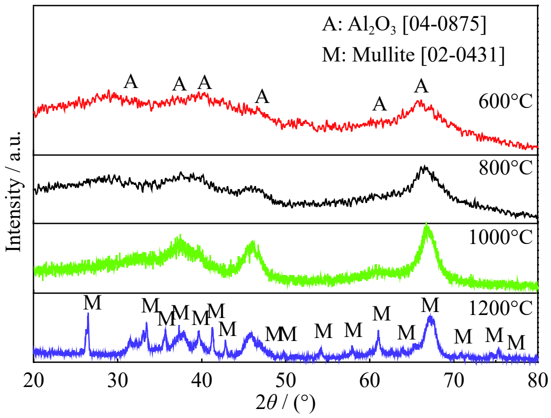

Fig. 1. XRD patterns of the as-prepared aerogels after firing at 600–1200°C.

dried one showed Si–OH stretching vibration at 956 cm^{-1}, confirming its existence in the gel network and verifying the reaction between TEOS and H_2O has taken place. When the temperature was increased to 800 and 1000°C, the Si–OH peaks (956 cm^{-1}) shifted towards 800 cm^{-1}, suggesting that the H atoms were gradually replaced by Si atoms in the network, forming the symmetric Si–O–Si bond [27]. This result proves that the Si–OH bond initially formed as early as in the drying stage and then transformed into Si–O–Si bond at later processing stages [38–39].

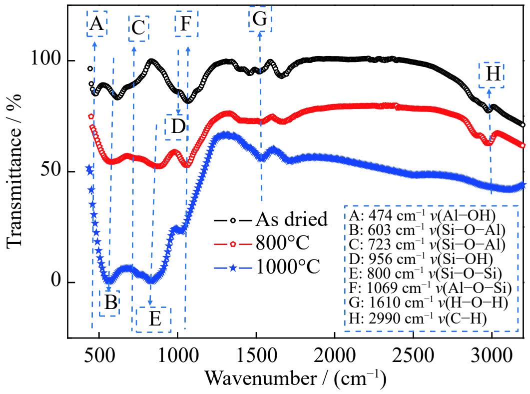

Fig. 2. FTIR of the as-prepared aerogels after drying and after firing at 800 and 1000°C (*v* is for stretching vibration).

On the other hand, Al–OH (474 cm^{-1}), Al–O (632 cm^{-1}), and Al−O−Al (1050 cm^{-1}, stretching vibration) were also detected, indicating the hydrolysis reaction between $AlCl_3\cdot6H_2O$ and PO has taken place [38–39]. Furthermore, some Al–O–Si (1069 cm^{-1}, stretching vibration [24]) bonds have also been detected when increasing temperature gradually. This result may be attributed to the condensation reactions between Al−OH and Si−OH/Si−OC_2H_5.

The presence of Al_2O_3 rather than SiO_2 in the XRD (Fig. 1) and FTIR (Fig. 2) results can be ascribed to the much faster gelation speed and larger composition quantity of the former than the latter [25]. In other words, as the Al−O−Al bond formed, the chance for Al–OH to react with Si–OH/Si–OC_2H_5 and form Al–O–Si bonds decreased. Hence, a mixture of mainly Al–O–Al and a possibly small amount of Si–O–Al was produced. Subsequently, Si–OH started to react with itself or Si−OC_2H_5, forming Si–O–Si. Consequently, SiO_2 and Si–O–Si were detected in the XRD and FTIR profiles (Figs. 1 and 2), respectively.

Other peaks, such as C–H (2990 cm^{-1}) and H–O–H (1610 cm^{-1}), were also observed in the as-dried and 800°C-heated samples, indicating that some organic solvents remained after the gelation/cross-linking process. When the temperature was increased to 1000°C, the –OH and C–H completely disappeared due possibly to the pyrolysis of these organics.

3.3. Microstructure

Fig. 3 shows that the as-prepared aerogels heated at 800°C are porous with pore diameters ranging from 10 to 20 nm and locating between the loosely packed nanoparticles (average diameters of 50–100 nm). The pores are quite homogeneous. Figs. 4(a) and 4(b) from two different locations both show that the as-prepared Al_2O_3–SiO_2 composite aerogels are needle-like and/or plate-like under a transmission electronic microscope, which is consistent with reference [40–41]. The Energy-dispersion X-ray spectroscopy (EDX) shows that the gels are composed of Al, Si, and O. This, together with the XRD and FTIR results, verifies the formation of Al_2O_3–SiO_2 composite aerogels. Element mapping (Figs. 3(d)–3(f)) shows that Al, Si, and O are presented homogeneously at identical positions in the aerogel. Overall, the PO-assisted sol–gel technique enabled the gelation better than traditional sol–gel techniques by avoiding the long pH adjustment procedures and controlling the hydrolysis rate [38–39].

3.4. Specific surface area and porosity

As seen from the adsorption–desorption loops (Fig. 5(a)), some clues can be drawn about the pore shapes from its H2 typed loops. These pore shapes might be stacking between the uniform nanoparticles, which is consistent with the SEM observations (Fig. 3). Furthermore, narrow distributions of pore sizes (Fig. 5(b)) were observed with the meso-pore sizes. The average diameters were 9.7, 13.4, 14.8, and 15.8 nm for the as-dried, 600°C-heated, 800°C-heated, and 1000°C-heated samples, respectively (Table 1).

Besides, Table 1 shows that the Barrett–Joyner–Halenda (BJH) specific surface area of the as-dried aerogel was 827.544 m^2/g, which was higher than those at 657.778, 455.839, and 225.984 m^2/g after heat treatment at 600, 800, and 1000°C, respectively. The Brunauer–Emmett–Teller (BET) specific surface area and the pore volume data are also shown in Table 1, suggesting that the aerogel sample has the highest total pore volume of ~1.46 mL/g after OSSD drying, dropping to 1.28, 1.08, and 0.59 mL/g after heat treatment at

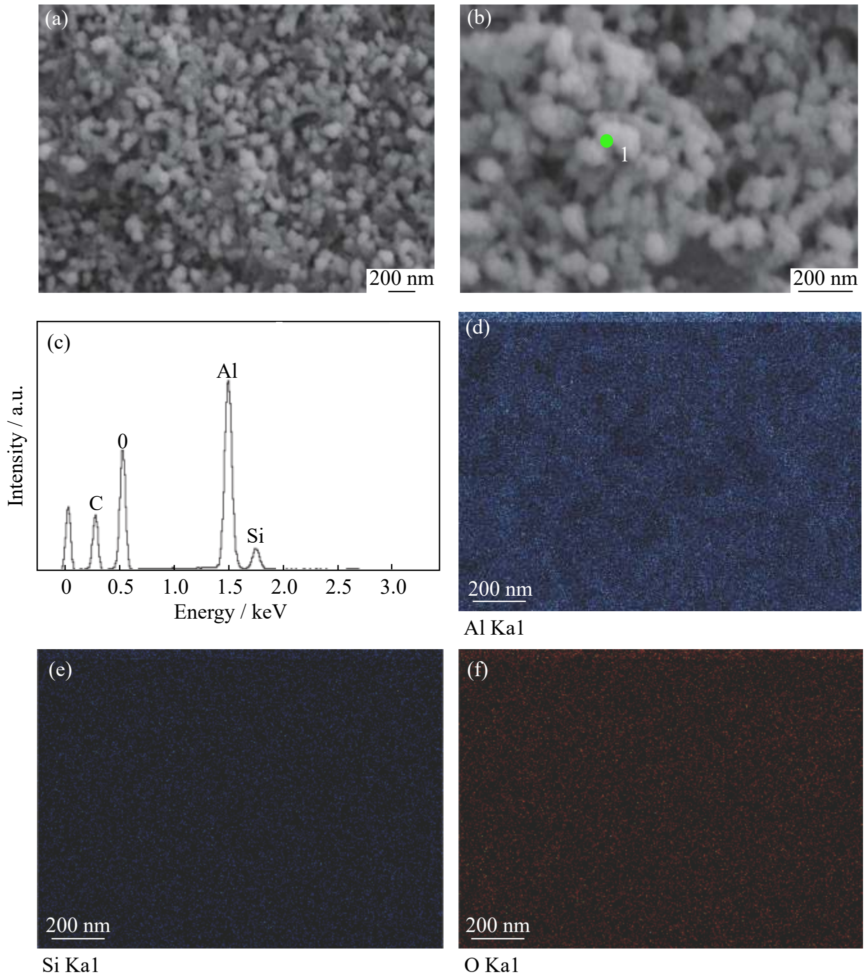

Fig. 3. SEM (a, b) of the Al_2O_3–SiO_2 composite aerogel, EDX (c) of point 1 in (b), and element mapping (d–f) corresponding to (b).

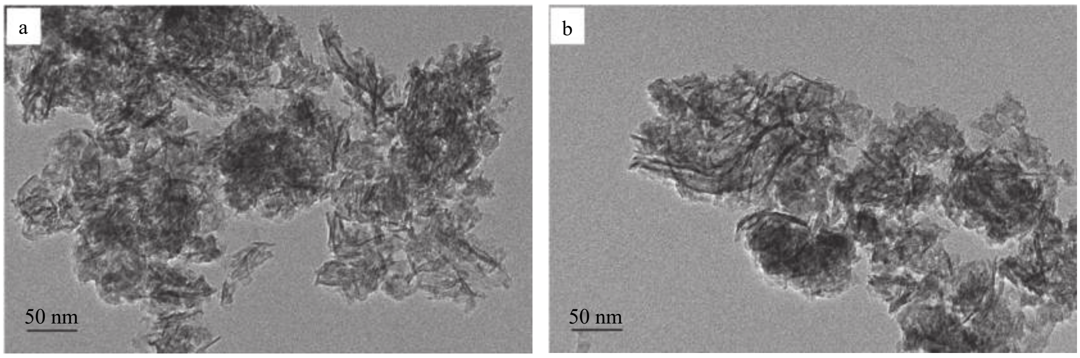

Fig. 4. Transmission electron microstructure of the Al_2O_3–SiO_2 composite aerogel heat treated at 800°C at two different locations (a) and (b).

600, 800, and 1000°C, respectively. The corresponding porosity was calculated as 86.0% for the as-dried sample, 83.6% for the 600°C-heated sample, 81.2% for the 800°C-heated sample, and 70.0% for the 1000°C-heated sample. These data indicate that the main component is Al_2O_3 (Fig. 1) and its density is ~3.9 g/cm^3. The porosity of this aerogel is up to 86.0%.

Such high surface areas and porosities can be possibly attributed to the OSSD drying method [11]. OSSD reduces the surface tensions and capillary forces between the aerogel channels and walls better than other drying methods [40]. It can also help the aerogel achieve relatively higher specific

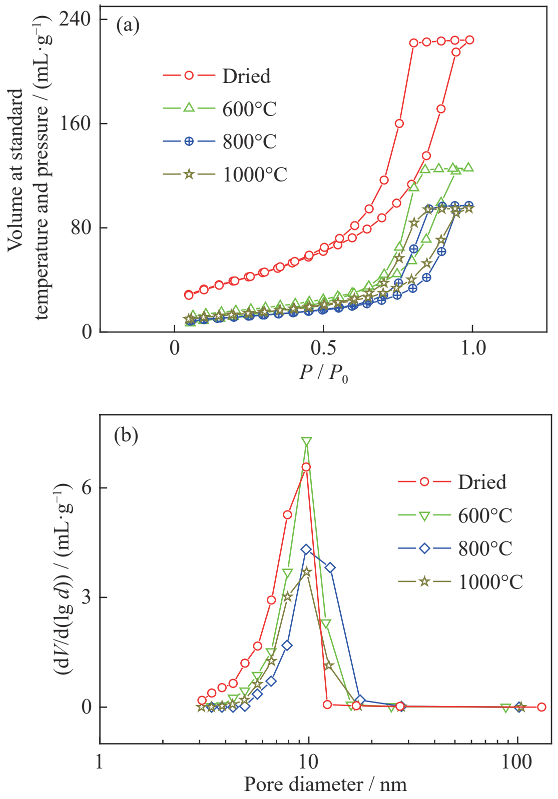

Fig. 5. Adsorption–desorption loop (a) and pore size distribution (b) of the aerogel after drying and firing at 600, 800, and 1000°C. P and P_0 stand for pressure at measurement and at standard temperature, respectively; V stands for the volume of absorbed N_2; d stands for pore diameter.

surface area and pore volume compared with previously reported aerogels (Table 2).

3.5. Cu^{2+} uptake by the Al_2O_3–SiO_2 composite aerogel

Preliminary tests were conducted on the absorption effect of aerogels on Cu^{2+}. In these spectra, the remaining concentration of Cu^{2+} dropped sharply within 40 min and reached ~0 afterward (Fig. 6(a)), and the removal efficiency can reach 99% in 40 min (Fig. 6(b)). In addition, the q_e (the absorption uptake at equilibrium) profile shows that the equilibrium Cu^{2+} uptake can reach ~69 mg/g (Fig. 6(c)). These results are better than those obtained in [11]. This high absorption efficiency can be possibly ascribed to the high surface area as shown in the BET and BJH specific surface area measurements (Fig. 5 and Table 1). Furthermore, it has easy accessible pores (Fig. 3) and high porosity (Table 1), which has greatly facilitated the diffusion of Cu^{2+} into bulk aerogel materials [11]. Finally, the multiple oxygen-containing functional groups (Al–OH, Si–OH, Al–O–Si, etc.) found in the composite aerogels (FTIR in Fig. 2) and the homogeneous distribution of Al, Si, and O (Fig. 3) might have afforded the aerogel excellent absorption properties [37]. The high surface area, easily accessible pores with high porosity, and oxygen-containing functional groups have synergistically promoted the absorption of Cu^{2+}.

Absorption kinetics was examined by performing the following calculations as previously described [11]. The absorption data of Cu^{2+} by the Al_2O_3–SiO_2 composite aerogels are consistent with the calculations from the pseudo second-order kinetics model ($R^2 = 0.9944$), which is much better than the pseudo first-order kinetics model ($R^2 = 0.8829$), as shown in Fig. 7. Therefore, the absorption process may follow the pseudo second-order kinetics and be controlled by the chemical absorption where valence forces and electron exchanges take charge [11].

The matches between the experimental and calculated data were evaluated using a normalized standard deviation Δq (%) [42], to validate the pseudo second-order model. The Δq (%) for the pseudo second-order model (82.55) fits more closely than the pseudo first-order one (148.83). Therefore, we speculated that the absorption of Cu^{2+} on the Al_2O_3–SiO_2 composite aerogel follows the pseudo second-order kinetics.

Table 1. Average pore diameters, total pore volume, porosity, and specific surface areas of the as-dried, 600°C-heated, 800°C-heated, and 1000°C-heated samples

Sample	Average pore diameters / nm	Total pore volume / ($mL\cdot g^{-1}$)	Porosity	BJH specific surface area / ($m^2\cdot g^{-1}$)	BET specific surface area / ($m^2\cdot g^{-1}$)
As-dried	9.7	1.46	86.0%	827.544	602.462
600°C	13.4	1.28	83.6%	657.778	381.520
800°C	14.8	1.08	81.2%	455.839	292.720
1000°C	15.8	0.59	70.0%	225.984	148.990

Table 2. Comparison between this work and references

Parameters	This work	References
Specific surface area	225.984 to 827.544 m^2/g	233.12–481.79 m^2/g [38] SiO_2 457.82 m^2/g and Al_2O_3 413.46 m^2/g [21]
Pore volume	0.6–1.5 mL/g	0.3–1.89 mL/g [40]

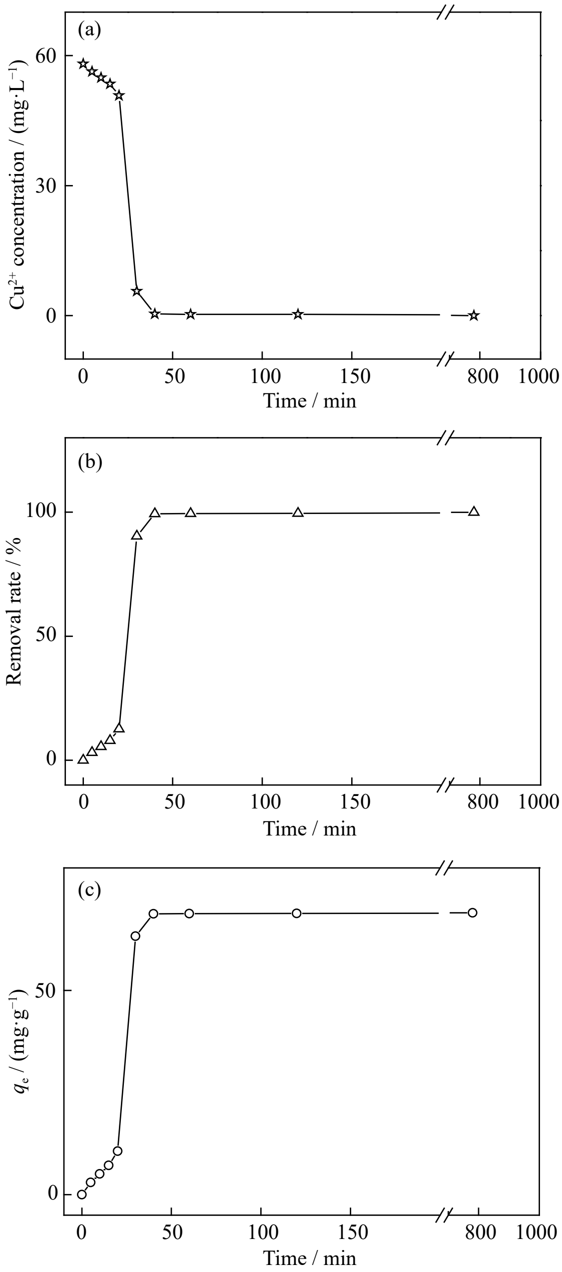

Fig. 6. Dependence of (a) Cu^{2+} concentration, (b) removal rate (%), and (c) uptake q_e on contact time.

4. Conclusion

Al_2O_3–SiO_2 composite aerogels were prepared using the PO-assisted sol−gel and OSSD methods. XRD and FTIR suggested that the aerogels are composed of mainly Al_2O_3 after firing below 1000°C. The aerogels have a high surface area of up to 827.544 m^2/g and high porosity of 86.0%. The H2 absorption/desorption loop and the SEM observations suggested that the pores are homogeneously located between the Al_2O_3–SiO_2 composite nanoparticles. The aerogels can absorb 99% Cu^{2+} (60 mg/L) in ~40 min and reach the equilibrium uptake at ~69 mg/g. Calculations showed that the absorption of the aerogels follows pseudo second-order kinetics. Such high efficiency can be attributed to the high specific surface areas, easy accessible microstructure with high porosity, and rich oxygen-containing functional groups in the aerogel network.

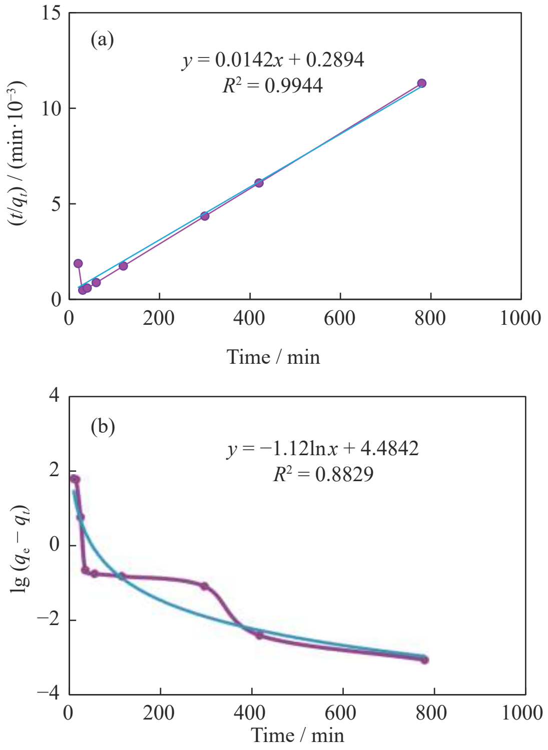

Fig. 7. Fit between the experimental Cu^{2+} absorption data and (a) pseudo second-order kinetics or (b) pseudo first-order kinetics. t is for absorption time; q_t and q_e stand for the uptake amount of Cu^{2+} per gram of the absorbent at time t and at equilibrium, respectively.

Acknowledgements

This work was financially supported by the National Natural Science Foundation of China (No. 51602018), the Beijing Municipal Natural Science Foundation (No. 2154052), the China Postdoctoral Science Foundation (No. 2014M560044), and the Fundamental Research Funds for the Central Universities, China (No. FRF-GF-17-B7).

References

[1] H. Maleki, Recent advances in aerogels for environmental remediation applications: A review, *Chem. Eng. J.*, 300(2016), p. 98.

[2] C. Santhosh, V. Velmurugan, G. Jacob, S.K. Jeong, A.N. Grace, and A. Bhatnagar, Role of nanomaterials in water treatment applications: A review, *Chem. Eng. J.*, 306(2016), p. 1116.

[3] M. Narayani and K.V. Shetty, Chromium-resistant bacteria and their environmental condition for hexavalent chromium remov-

al: A review, *Crit. Rev. Environ. Sci. Technol.*, 43(2013), No. 9, p. 955.

[4] F. Gode and E. Pehlivan, Removal of chromium(III) from aqueous solutions using Lewatit S 100: The effect of pH, time, metal concentration and temperature, *J. Hazard. Mater.*, 136(2006), No. 2, p. 330.

[5] F.L. Fu and Q. Wang, Removal of heavy metal ions from wastewaters: A review, *J. Environ. Manage.*, 92(2011), No. 3, p. 407.

[6] L.B. Hoch, E.J. Mack, B.W. Hydutsky, J.M. Hershman, J.M. Skluzace, and T.E. Mallouk, Carbothermal synthesis of carbon-supported nanoscale zero-valent iron particles for the remediation of hexavalent chromium, *Environ. Sci. Technol.*, 42(2008), No. 7, p. 2600.

[7] D. Yang, X.Y. Zhao, X.Y. Zou, Z.Y. Zhou, and Z.Y. Jiang, Removing Cr(VI) in water via visible-light photocatalytic reduction over Cr-doped $SrTiO_3$ nanoplates, *Chemosphere*, 215(2019), p. 586.

[8] J. Li, X.X. Wang, G.X. Zhao, C.L. Chen, Z.F. Chai, A. Alsaedi, T. Hayat, and X.K. Wang, Metal-organic framework-based materials: Superior adsorbents for the capture of toxic and radioactive metal ions, *Chem. Soc. Rev.*, 47(2018), No. 7, p. 2322.

[9] A.E. Burakov, E.V. Galunin, I.V. Burakova, A.E. Kucherova, S. Agarwall, A.G. Tkachev, and V.K. Gupta, Adsorption of heavy metals on conventional nanostructured materials for waste water treatment purposes: A review, *Ecotoxicol. Environ. Saf.*, 148(2018), p. 702.

[10] Q.X. Zheng, Li Z.L., X.X. Miao, Li J.H., Y.F. Huang, H.N. Xia, and C.H. Xiong, Preparation and characterization of novel organic chelating resin and its application in recovery of Zn(II) from aqueous solutions, *Appl. Organomet. Chem.*, 31(2017), art. No. e3546.

[11] X. Mi, G.B. Huang, W.S. Xie, W. Wang, Y. Liu, and J.P. Gao, Preparation of graphene oxide aerogel and its adsorption for Cu^{2+} ions, *Carbon*, 50(2012), No. 13, p. 4856.

[12] K. Vikrant and K.H. Kim, Nano-materials for the adsorptive treatment of Hg(II) ions from water, *Chem. Eng. J.*, 358(2019), p. 264.

[13] Y.B. Sun, S.B. Yang, Y. Chen, C.C. Ding, W.C. Cheng, and X.K. Wang, Adsorption and desorption of U(VI) on functionalized graphene gxides: A combined experimental and theoretical study, *Environ. Sci. Technol.*, 49(2015), No. 7, p. 4255.

[14] B. Cai, V. Sayevich, N. Gaponik, and A. Eychmuller, Emerging hierarchical aerogels: Self-assembly of metal and semiconductor nanocrystals, *Adv. Mater.*, 30(2018), No. 33, art. No. 1707518.

[15] M. Moner-Girona, A. Roig, E. Molins, and J. Llibre, Sol–gel route to direct formation of silica aerogel microparticles using supercritical solvents, *J. Sol Gel Sci. Technol.*, 26(2003), No. 1, p. 645.

[16] T.F. Baumann, A.E. Gash, S.C. Chinn, A.M. Sawvel, R.S. Maxwell, and. J.H. Satcher, Synthesis of high-surface-area alumina aerogels without the use of alkoxide precursors, *Chem. Mater.*, 17(2005), No. 2, p. 395.

[17] L.B. Hammouda, I. Mejri, M.K. Younes, and A. Ghorbel, ZrO_2 aerogels, [in] M.A. Aegerter, N. Leventis, and M.M. Koebel, eds., *Aerogels Handbook*, Springer, New York, 2011, p. 127.

[18] H. Hirashima, Preparation of TiO_2 aerogels-like materials under ambient pressure, [in] M.A. Aegerter, N. Leventis, and M.M. Koebel, eds., *Aerogels Handbook*, Springer, New York, 2011, p. 145.

[19] A.C. Pierre and A. Rigacci, SiO_2 aerogels, [in] M.A. Aegerter, N. Leventis, and M.M. Koebel, eds., *Aerogels Handbook*, Springer, New York, 2011, p. 21.

[20] A.M. Anderson and M.K. Carroll, Hydrophobic silica aerogels: Review of synthesis, properties and applications, [in] M.A. Aegerter, N. Leventis, and M.M. Koebel, eds., *Aerogels Handbook*, Springer, New York, 2011, p. 47.

[21] S. Mulik and C. Sotiriou-Leventis, Resorcinol-formaldehyde aerogels, [in] M.A. Aegerter, N. Leventis, and M.M. Koebel, eds., *Aerogels Handbook*, Springer, New York, 2011, p. 215.

[22] A. Rigacci and P. Achard, Cellulosic and polyurethane aerogels, [in] M.A. Aegerter, N. Leventis, and M.M. Koebel, eds., *Aerogel Handbook*, Springer, New York, 2011, p. 191.

[23] T. Horikawa, J. Hayashi, and K. Muroyama, Size control and characterization of spherical carbon aerogel particles from resorcinol-formaldehyde resin, *Carbon*, 42(2004), No. 1, p. 169.

[24] M.A. Worsley, J.H. Satcher Jr., and T.F. Baumann, Synthesis and characterization of monolithic carbon aerogel nanocomposites containing double-walled carbon nanotubes, *Langmuir*, 24(2008), No. 17, p. 9763.

[25] M.A. Worsley, P.J. Pauzauskie, T.Y. Olson, J. Biener, J.H. Satcher Jr., and T.F. Baumann, Synthesis of graphene aerogel with high electrical conductivity, *J. Am. Chem. Soc.*, 132(2010), No. 40, p. 14067.

[26] D.C. Wu, F. Xu, B. Sun, R.W. Fu, H.K. He, and K. Matyjaszewski, Design and preparation of porous polymers, *Chem. Rev.*, 112(2012), No. 7, p. 3959.

[27] S.L. Brock and H.T. Yu, Chalcogenide aerogels, [in] M.A. Aegerter, N. Leventis, and M.M. Koebel, eds., *Aerogels Handbook*, Springer, New York, 2011, p. 367.

[28] J.L. Mohanan, I.U. Arachchige, and S.L. Brock, Porous semiconductor chalcogenide aerogels, *Science*, 307(2005), No. 5708, p. 397.

[29] G.Q. Zu, J. Shen, W.Q. Wang, L.P. Zou, Y. Lian, Z.H. Zhang, B. Liu, and F. Zhang, Robust, highly thermally stable, core-shell nanostructured metal oxide aerogels as high-temperature thermal superinsulators, adsorbents, and catalysts, *Chem. Mater.*, 26(2014), No. 19, p. 5761.

[30] T.W. Wang, H. Sun, J.W. Long, Y.Z. Wang, and D. Schiraldi, Biobased poly(furfuryl alcohol)/clay aerogel composite prepared by a freeze-drying process, *ACS Sustainable Chem. Eng.*, 4(2016), No. 5, p. 2601.

[31] Y.L. Pan, X.D. Cheng, T. Zhou, L.L. Gong, and H.P. Zhang, Spray freeze-dried monolithic silica aerogel based on waterglass with thermal super-insulating properties, *Mater. Lett.*, 229(2018), p. 265.

[32] L.L. Ren, S.M. Cui, F.C. Cao, and Q.H. Guo, An easy way to prepare monolithic inorganic oxide aerogels, *Angew. Chem. Int. Ed.*, 53(2014), No. 38, p. 10147.

[33] J.J. Liao, P.Z. Gao, L. Xu, and J. Feng, A study of morphological properties of SiO_2 aerogels obtained at different temperatures, *J. Adv. Ceram.*, 7(2018), No. 4, p. 307.

[34] L.Y. Yu, Z.L. Xu, H.M. Shen, and H. Yang, Preparation and characterization of PVDF-SiO_2 composite hollow fiber UF membrane by sol–gel method, *J. Membr. Sci.*, 337(2009), No. 1-2, p. 257.

[35] A.S.M. Chong and X.S. Zhao, Functionalization of SBA-15 with APTES and characterization of functionalized materials, *J. Phys. Chem. B*, 107(2003), No. 46, p. 12650.

[36] D. Janackovic, V. Jakanovic, L. Kostic-Gvozdenovic, and D. Uskokovic, Synthesis of mullite nanostructured spherical powder by ultrasonic spray pyrolysis, *Nanostruct. Mater.*, 10(1998), No. 3, p. 341.

[37] M. Medina, J. Tapia, S. Pacheco, M. Espinosa, and R. Rodriguez, Adsorption of lead ions in aqueous solution using silica-

alumina nanoparticles, *J. Non-Cryst. Solids*, 356(2010), No. 6-8, p. 383.

[38] X.F. Ji, Q. Zhou, G.B. Qiu, B. Peng, M. Guo, and M. Zhang, Synthesis of an alumina enriched Al_2O_3–SiO_2 aerogel: Reinforcement and ambient pressure drying, *J. Non-Cryst. Solids*, 471(2017), p. 160.

[39] S.J. Juhl, N.J.H. Dunn, M.K. Carroll, A.M. Anderson, B.A. Bruno, J.E. Madero, and M.S. Bono Jr., Epoxide-assisted alumina aerogels by rapid supercritical extraction, *J. Non-Cryst. Solids*, 426(2015), p. 141.

[40] A.S. Shaygin, I.V. Kozhevnikov, E.Y. Gerasimov, A.S. Andreev, O.B. Lapina, and O.N. Martyanov, The impact of Si/Al ratio on properties of aluminosilicate aerogels, *Microporous Mesoporous Mater.*, 251(2017), p. 105.

[41] X.D. Wu, G.F. Shao, S. Cui, L. Wang, and X.D. Shen, Synthesis of a novel Al_2O_3–SiO_2 composite aerogel with high specific surface area at elevated temperatures using inexpensive inorganic salt of aluminum, *Ceram. Int.*, 42(2016), No. 1, p. 874.

[42] L. Wang, J. Zhang, R. Zhao, Y. Li, C. Li, and C.L. Zhang, Adsorption of Pb(II) on activated carbon prepared from *Polygonum orientale* Linn.: Kinetics, isotherms, pH, and ionic strength studies, *Bioresource Technol.*, 101(2010), No. 15, p. 5808.